High Energy Density Physics 36 (2020) 100837

Contents lists available at ScienceDirect

High Energy Density Physics

journal homepage: www.elsevier.com/locate/hedp

# Flash X-ray backlight technique using a Fresnel phase zone plate for measuring interfacial instability

Kazuki Matsuo*[,a], Takayoshi Sano[a], Kazuki Ishigure[a], Hiroki Kato[a], Natsuko Nagamatsu[b], Zhu Baojun[a], Guo Shuwang[a], Hideo Nagatomo[a], Nicolai Philippe[c], Youichi Sakawa[a], Yasunobu Arikawa[a], Shohei Sakata[a], SeungHo Lee[a], King Fai Farley Law[a], Hiroki Morita[a], Chang Liu[a], Huan Li[a], Jo Nishibata[a], Ryunosuke Takizawa[a], Hiroshi Azechi[a], Shinsuke Fujioka*[,a]

[a] Institute of Laser Engineering, Osaka University, 2-6 Yamada-oka, Suita, Osaka, Japan
[b] Nanotechnology Hub, Kyoto-University, Japan
[c] CELIA University Bordeaux, France

ARTICLE INFO

*Keywords:*
Flash X-ray backlighting
Fresnel phase zone plate
Interfacial instability

ABSTRACT

Interfacial instabilities in high-energy-density plasmas are important topics in various research fields such as inertial confinement fusion, planetary sciences, and astrophysics. The growth of the instabilities can be examined in the laboratory by using high-power lasers coupled with high-resolution imaging technique. The resolutions both in space and time are essential for the observation of tiny and transient phenomena in high-energy-density plasmas. Here, the growth of a sinusoidal corrugation on the surface of a polystyrene foil during the laser-driven Richtmyer-Meshkov instability was measured by high-resolution X-ray shadowgraphy. In our experiment, a high-intensity short-pulse laser produced the X-ray flash that ensures a better temporal resolution. A Fresnel Phase Zone Plate was used for the improvement of spatial resolution, which realized an accuracy of 5.0 ± 1.0 μm in our system.

## 1. Introduction

The interfacial instabilities, i.e. Rayleigh-Taylor [1,2], Richtmyer-Meshkov (RM) [3,4], and Kelvin-Helmholtz [5,6] instabilities, are phenomena observed widely in planetary science, astrophysics, and fusion plasmas. Especially understanding of the interfacial instability in high-energy-density plasma is of great importance in the fields of astrophysical fluid dynamics [7] as well as toward the achievement of the inertial confinement fusion ignition [8]. High power laser facilities can drive the interfacial instabilities in high-energy-density plasmas. One of the approaches to access the interfacial instabilities in the laboratory is to measure the shadow of the interface with spatially and temporally resolved imaging technique, which is essential in high-energy-density plasma experiment because the phenomena are tiny and transient.

A pinhole is frequently used as an X-ray imager in high-energy-density plasma experiment for measuring the shadow of the interface [9–11]. The X-ray pinhole is easy to set up and relatively low operating costs. However, the resolution is limited by the pinhole diameter, and the light collection angle is reduced by increasing the resolution. Since the pinhole method does not have any wavelength selectivity, filtering is required to obtain a quasi-monochromatic image. It is impossible to select a narrow bandwidth without significant signal loss due to the filtering.

Diffractive optics for imaging a hard X rays was proposed in 1963 [12]. This optics is now known as the Fresnel phase zone plate (FPZP), which is used for focusing and imaging hard X rays. Like pinhole, the FPZP works with less geometrical restrictions compared to other X-ray optics. The FPZP is not frequently used in high-energy-density plasma experiment due to the expensive cost for manufacturing. The FPZP can provide high spatial resolution X-ray images without sacrificing the collection angle owing to the larger diameter with precision manufacturing of thin rings. The demonstration of FPZP as a high-resolution imager in high-energy-density plasma experiment has been reported in Ref. [13]. The experiment was performed at the LULI2000 laser facility to image Al-He$_\beta$ emitted from a laser-produce plasma. It is demonstrated that the FPZP can provide a reusable and high-resolution X-ray microscope for high-energy-density plasma experiment diagnostic.

In this study, we have tested the FPZP coupled with flash X-ray backlight technique [14,15] at the GEKKO-LFEX laser facility at the Institute of Laser Engineering, Osaka University. A sinusoidally

* Corresponding authors.
*E-mail addresses:* matsuo-k@ile.osaka-u.ac.jp (K. Matsuo), matsuo-k@ile.osaka-u.ac.jp (S. Fujioka).

https://doi.org/10.1016/j.hedp.2020.100837
Received 12 February 2020; Received in revised form 29 May 2020; Accepted 29 May 2020
Available online 01 June 2020
1574-1818/ 

**Table 1**
Parameters of the FPZP used in this experiment.

| Material | Tantalum |
|---|---|
| Radius of the innermost annular slit ($a$) | 6 μm |
| Radius of the outermost annular slit ($d$) | 52 μm |
| Thickness | 1 ± 0.1 μm |
| Last zone width | 0.15 ± 0.03 μm |

corrugated polystyrene foil was irradiated by nanosecond GEKKO-XII beams to drive the RM instability. Ti-$K_\alpha$ X-ray flash was produced by irradiating a titanium foil with high-intensity picosecond LFEX laser. The flash X rays pass through the sinusoidally corrugated polystyrene foil was imaged with the FPZP on an imaging plate in the edge-on backlight geometry. We demonstrated 5.0 ± 1.0 μm of spatial resolution with the developed imaging system. Perturbation amplification caused by the RM instability was observed successfully in this experiment.

## 2. Imaging principle of X-ray Fresnel phase zone plate

The FPZP has a function to converge a part of a planar X-ray wave to the focal point. The FPZP used in this study consists of concentered multiple annular slits made in a 1 μm-thickness Tantalum membrane. The distances between adjacent slits are designed to give 2π radians of the phase difference between wavelets passing through the slits at the focal point. The thickness of the tantalum membrane is designed to add π radians phase to a transmit wavelet compared to that passing through the slits. Therefore the phase difference between a wavelet passing through a membrane bar and an adjacent slit is 2π at the focal point. Finally, all wavelets passed through the FPZP interfere constructively with each other at the focal point.

The focal length of FPZP is $f = a^2/\lambda$, here $a$ and λ are the radius of the innermost annular slit and a wavelength of light, respectively. The focal length determines the relation between a distance from the objective to the FPZP ($r$) and that from the FPZP to the image plane ($R$) as a normal lens as,

$$\frac{1}{f} = \frac{1}{r} + \frac{1}{R}. \tag{1}$$

Since the focal length is a function of the wavelength, the focal position of out-of-band radiation is different from that of in-band radiation, and the image of the out-of-band radiation is not formed on the designed image plane. By reducing the radius of the innermost annular slit, it is possible to focus the X rays at a closer position to the target. This feature is useful when the experimental space is physically limited. The fabrication parameters of the FPZP are listed in Table 1. The radius of the innermost annular slit $a$ of the FPZP was 6 μm, and then the focal distance for Ti-$K_\alpha$ X rays was 131 mm.

Fig. 1 (a) shows the schematics of FPZP imaging. When the monochromatic parallel X-ray beam incident to the FPZP, the 1st order light is focused at the focal point on the image plane. The 0th, 3rd, and higher odd orders of unfocused lights also come to the image plane. The efficiency of the $k$th order light can be calculated with the following equations [16].

$$\eta_0 = \frac{1}{4}\left(1 + 2e^{\frac{-2\pi\beta e}{\lambda}}\cos\left(\frac{-2\pi\delta e}{\lambda}\right) + e^{\frac{-4\pi\beta e}{\lambda}}\right) \tag{2}$$

$$\eta_k = \frac{1}{\pi^2 k^2}\left(1 - 2e^{\frac{-2\pi\beta e}{\lambda}}\cos\left(\frac{-2\pi\delta e}{\lambda}\right) + e^{\frac{-4\pi\beta e}{\lambda}}\right) \tag{3}$$

Here $\delta$ and $\beta$ are the real and imaginary parts of the refractive index of the membrane material $n = 1 - \delta - i\beta$. Henke's table [17] was used for obtaining $\delta$ and $\beta$. Using these formulas, we select the thickness to maximize the ratio of the 1st order over the other orders. Fig. 1(b) shows a comparison of the efficiencies of the 0th, 1st, and 3rd orders for 1 μm-thick tantalum. The efficiency of the 0th and 3rd orders around Ti-$K_\alpha$(= 4510 eV) X rays is small compare to that of the 1st order. The 0th-order efficiency is dominant in the hard X-ray range over 7000 eV, where the 1 μm-thickness Tantalum membrane does not diffract the X rays. Although these rays are not focused at an identical point but spread on a large area, they could cause background noises at the focal plane. This could be a factor that determines the applicable range of the plasma to be measured by using the FPZP.

It is difficult to produce a monochromatic X rays from laser-produced plasma. Fig. 2(a) shows an X-ray spectrum from laser-irradiated titanium foil which is calculated by FLYCHK code [18] in the range of 4300 to 4900 eV. In this calculation, we used parameters that are evaluated from our previous experiment [19]; bulk plasma electron temperature and density are 1 keV and $10^{23}$ cm$^{-3}$, and hot electron slope temperature and density are 1 MeV and $10^{19}$ cm$^{-3}$, respectively. The peaks at 4510 and 4750 are Ti-$K_\alpha$ and Ti-$He_\alpha$ respectively. Even in this situation, the FPZP can provide high spatial resolution X-ray images owing to their wavelength selectivity. The intensity of point source X rays focused on the image plane $I(\sigma)$ can be calculated by the following equation of the Fresnel diffraction.

$$\frac{4\pi^2}{(rR\lambda)^2}\left|\int_0^d \rho\exp\left(\frac{i\pi(R+r)\rho^2}{rR\lambda}\right)J_0\left(\frac{2\pi\sigma\rho}{R\lambda}\right)d\rho\right|^2 \tag{4}$$

where $\sigma$ is a distance from center of the image plane, ρ is a distance from center of the FPZP, $d$ is a radius of the outermost annular slit, which are the measured values of a manufactured plate listed in Table 1. The X-ray intensity is calculated from Eq. (4) with various X-ray energy, as shown in Fig. 2(b). The object to FPZP distance $r$ and the

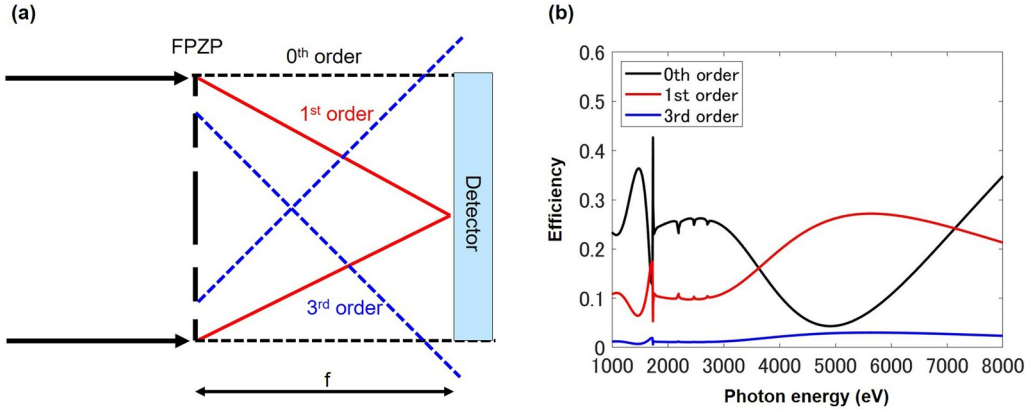


**Fig. 1.** (a) Schematics of FPZP imaging, showing rays of the various diffraction orders. (b) Efficiency of the 0th, 1st, and 3rd orders of the FPZP calculated by Eqs. (2) and (3).

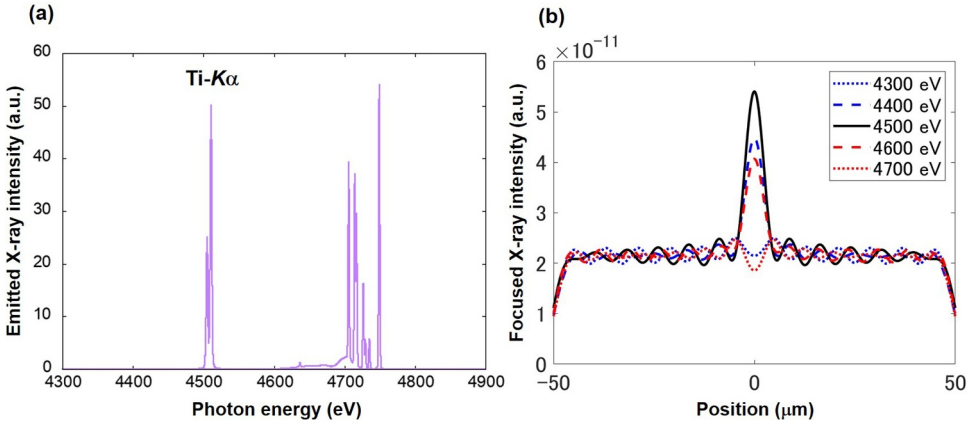


**Fig. 2.** (a) An example of X-ray spectrum emitted from a laser-produced titanium plasma. (b) Point spread functions calculated for different X-ray energies.

FPZP to the image plane distance $R$ are 144 mm and 1440 mm, respectively. Ti-$K_\alpha$ X rays are well focused on the image plane. Although other X rays near Ti-$K_\alpha$ line are also focused on the detector, there are no strong characteristic X-ray emissions around Ti-$K_\alpha$ line. It is important to reduce chromatic aberration. To avoid the influence of the self-emission, we should select higher X-ray photon energy than dominant one of the self-emission for the backlighting. On the other hand, it is difficult to make a shadow on a detector because of its high transmittance if the X-ray photon energy is too high. From the previous study [20], Ti-$K_\alpha$ X-ray energy is enough higher than dominant X-ray photon energy of the self-emission and suitable to create shadows with the target used in this experiment.

## 3. X-ray backlight imaging with FPZP and X rays produced by short pulse laser

The spatial resolution of the imaging system was evaluated by using a gold mesh backlit by Ti-$K_\alpha$ X rays. The experimental setup is illustrated in Fig. 3(a). The LFEX laser for backlighting was 1.6 ps of the pulse duration. The total energy of 1 kJ was focused on a titanium foil for producing flash Ti-$K_\alpha$ X rays. The Ti-$K_\alpha$ X rays passed through a gold mesh and imaged on an image plate (IP) detector (IP type: BAS-MS). After data acquisition, the IP was scanned with the Typhoon FLA7000 scanner at a spatial resolution of 25 μm. A 50-μm-thick beryllium foil was placed in front of the FPZP for protecting the FPZP from debris. Then the FPZP was undamaged by the shot and reusable in our

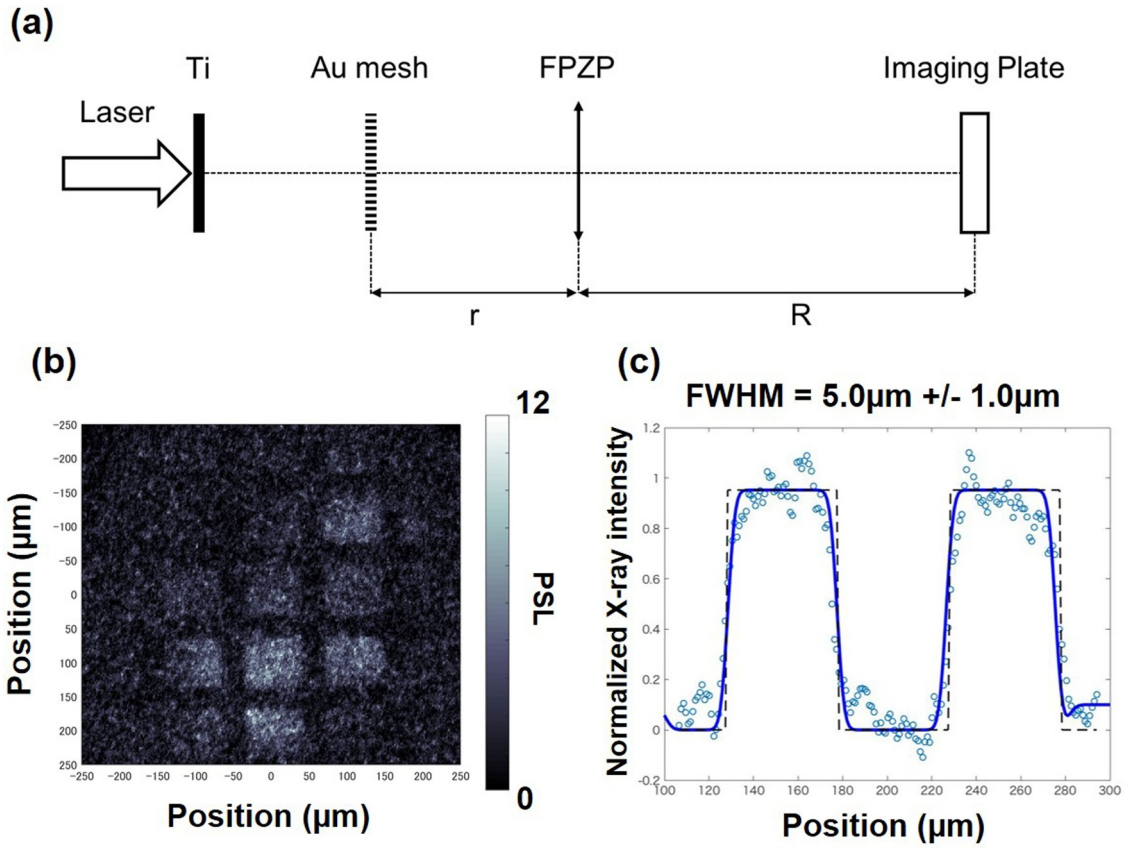


**Fig. 3.** (a) Experimental setup of the backlight imaging experiment. (b) X-ray radiograph of the gold mesh backlight by the Ti$K_\alpha$ X rays. (c) Line profile of individual pixels of the measured backlight image (dot) and a calculated profile (solid line) obtained by convoluting an ideal profile (dotted line) and a Gaussian point spread function 5.0 μm of FWHM.

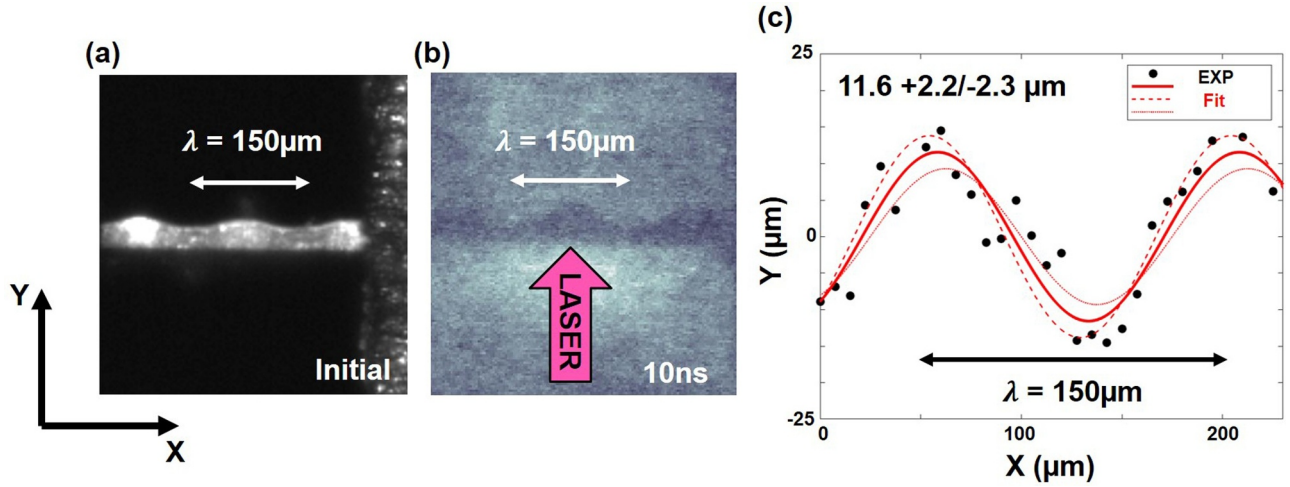


**Fig. 4.** (a) A photograph of sinusoidally corrugated polystyrene foil. (b) The shadow measured by flash X-ray backlight technique using FPZP after 10 ns laser irradiation. (c) Profile of rear surface and fitting curves of sinusoidal perturbation for 11.6 + 2.2/−2.3 μm amplitude.

experiment. The backlight image of the gold mesh was shown in Fig. 3(b). The line profile of individual pixels of the measured backlight image is shown with the dots in Fig. 3(c). The dotted and solid lines in Fig. 3(c) are the ideal line profile of the backlight image and the calculated profile obtained by convoluting the ideal image and a Gaussian point spread function. This comparison indicates that the spatial resolution at FWHM is $\delta = 5.0 \pm 1.0$ μm. The FPZP must be placed at the desired position with accuracy of ± 0.72 mm for achieving 5 μm of spatial resolution. We attached a needle, whose length was pre-measured with accuracy of 0.1 mm, at the tip of an FPZP positioner nose. The length of the nose was adjusted to put the needle tip at the target chamber center, this needle was removed after this adjustment.

RM instabilities, which has been well studied theoretically [21,22] and experimentally [23,24] in high-energy-density plasmas, was measured with the imaging system. A 150 μm wavelength sinusoidal perturbation with the initial amplitude 7.9 ± 0.5 μm was imposed on the rear surface of a planar polystyrene foil, whose thickness was 50 μm, as shown in Fig. 4(a). Two 532 nm beams of the GEKKO-XII laser were used to drive the foil at an intensity of $(4.0 \pm 0.1) \times 10^{13}$ W/cm$^2$ from the front surface. The RM instability occurs at the foil-vacuum boundary when an incident shock strikes the corrugated density boundary. The perturbation growth is excited by the vorticity deposited at the interface. The shadow was measured by flash X-ray backlight technique using the FPZP at 10 ns after the GEKKO-XII laser irradiation, as shown in Fig. 4(b). Although the temporal duration of Ti-$K_\alpha$ pulse produced by the LFEX laser was not measured in this experiment, according to previous theoretical study [25], it is reasonable to assume that the duration of the X-ray pulse is of the order of 1.6 ps. It enables to record an instantaneous image of the sinusoidal perturbation, in which the blur due to hydrodynamic motions is negligibly small. The width of the polystyrene foil along the line of sight of the diagnostics was $l$= 400 μm, and thus the transmittance of Ti-K$_\alpha$ X rays is 0.35 for the initial polystyrene density (1.1 g/cm$^3$). The target boundary was defined by the transmittance line. Fig. 4(c) shows the trace of the rear surface of the target. The evaluated amplitude is $11.6^{+2.2}_{-2.3}$ μm at 10 ns after the laser irradiation. The quality of the obtained images suggests that the instability growth can be observable in our setup even under the influence of self-emission from the plastic foil.

## 4. Conclusion

In this study, we used the FPZP coupled with flash X-ray backlight technique [14,15] at the GEKKO-LFEX laser facility. We demonstrated that 5.0 ± 1.0 μm of spatial resolution with the developed imaging system. The imaging system has successfully captured the perturbation growth caused by the RM instability. The FPZP coupled with flash X-ray shadowgraphy is one of the approaches to access the interfacial instabilities in the laboratory with spatially and temporally high-resolution.

## Declaration of Competing Interest

To the best of our knowledge, the named authors have no conflict of interest, financial or otherwise.

## Acknowledgements

The authors thank the technical support staffs of ILE at Osaka University for assistance with laser operation, target fabrication, and plasma diagnostics. This work was supported by Kyoto University Nanotechnology Hub in Nanotechnology Platform Project sponsored by the Ministry of Education, Culture, Sports and Technology (MEXT), NFP-18-010 Japan. This work was supported by the Collaboration Research Program between the National Institute for Fusion Science and the Institute of Laser Engineering at Osaka University (NIFS12KUGK057, NIFS15KUGK087, NIFS17KUGK111, and NIFS18KUGK118) This work is supported by Institute of Laser Engineering, Osaka University through collaboration research program, and the Japanese Ministry of Education, Science, Sports, and Culture through Grants-in-Aid, KAKENHI (15KK0163, 16H02245, and 16K13918 ) and Grant-in-Aid for Fellows by Japan Society for The Promotion of Science (Grant nos. 18J11354 and 18J11119), the Matsuo Research Foundation and Research Foundation for Opto-Science and Technology.

## References

[1] L. Rayleigh, Investigation of the character of the equilibrium of an incompressible heavy fluid of variable density, Proc. Lond. Math. Soc. 14 (1883) 170–177.
[2] G.I. Taylor, The instability of liquid surfaces when accelerated in a direction perpendicular to their planes, Proc. R. Soc. Lond. Ser. A 201 (1950) 159–174.
[3] R.D. Richtmyer, Taylor instability in shock acceleration of compressible fluids, Commun. Pure Appl. Math. 13 (2) (1960), https://doi.org/10.1002/cpa.3160130207.
[4] E.E. Meshkov, Instability of the interface of two gases accelerated by a shock wave, Fluid Dyn. 4 (5) (1969), https://doi.org/10.1007/BF01015969.
[5] W. Thomson, Hydrokinetic solutions and observations, Philos. Mag. 42 (1871) 362–377.
[6] H. von Helmholtz, On the discontinuous movements of fluid, Philos. Mag. 36 (1868) 337–346.
[7] B.A. Remington, R.P. Drake, D.D. Ryutov, Experimental astrophysics with high power lasers and Z pinches, Rev. Mod. Phys. 78 (3) (2006), https://doi.org/10.1103/RevModPhys.78.755.
[8] R. Betti, O.A. Hurricane, Inertial-Confinement fusion with lasers, Nat. Phys. 12 (5)

(2016), https://doi.org/10.1038/NPHYS3736.
[9] C.C. Kuranz, B.E. Blue, R.P. Drake, H.F. Robey, J.F. Hansen, J.P. Knauer, M.J. Grosskopf, C. Krauland, D.C. Marion, Dual, orthogonal, backlit pinhole radiography in OMEGA experiments, Rev. Sci. Instrum. 77 (10) (2006), https://doi.org/10.1063/1.2351870.
[10] F.W. Doss, E.N. Loomis, L. Welser-Sherrill, J.R. Fincke, K.A. Flippo, P.A. Keiter, Instability, mixing, and transition to turbulence in a laser-driven counterflowing shear experiment, Phys. Plasmas 20 (1) (2013), https://doi.org/10.1063/1.4789618.
[11] S.R. Nagel, K.S. Raman, C.M. Huntington, S.A. Maclaren, P. Wang, M.A. Barrios, T. Baumann, J.D. Bender, L.R. Benedetti, D.M. Doane, S. Felker, P. Fitzsimmons, K.A. Flippo, J.P. Holder, D.N. Kaczala, T.S. Perry, R.M. Seugling, L. Savage, Y. Zhou, A platform for studying the Rayleigh-Taylor and Richtmyer-Meshkov instabilities in a planar geometry at high energy density at the national ignition facility, Phys. Plasmas 24 (7) (2017), https://doi.org/10.1063/1.4985312.
[12] Y.N. Denisiuk, On the reflection of the optical properties of object in optical field scattered on it, Opt. Spectrosc. 15 (1963) 522.
[13] A. Do, P. Troussel, S.D. Baton, V. Dervieux, D. Gontier, L. Lecherbourg, B. Loupias, L. Obst, F. Pérez, P. Renaudin, C. Reverdin, C. Rubbelynck, P. Stemmler, G. Soullié, High-resolution quasi-monochromatic X-ray imaging using a Fresnel phase zone plate and a multilayer mirror, Rev. Sci. Instrum. 88 (2017), https://doi.org/10.1063/1.4973296.
[14] S. Fujioka, T. Fujiwara, M. Tanabe, H. Nishimura, H. Nagatomo, S. Ohira, Y. Inubushi, H. Shiraga, H. Azechi, Monochromatic x-ray radiography for areal-density measurement of inertial fusion energy fuel in fast ignition experiment, Rev. Sci. Instrum. 81 (10) (2010), https://doi.org/10.1063/1.3494383.
[15] H. Sawada, S. Lee, T. Shiroto, H. Nagatomo, Y. Arikawa, H. Nishimura, T. Ueda, K. Shigemori, A. Sunahara, N. Ohnishi, F.N. Beg, W. Theobald, F. Pérez, P.K. Patel, S. Fujioka, Flash Kα radiography of laser-driven solid sphere compression for fast ignition, Appl. Phys. Lett. 108 (25) (2016), https://doi.org/10.1063/1.4954383.
[16] T. G.Brown, (2004) The Optics EncyclopediaVol. 5 ISBN: 978-3-527-40320-2 Publisher: Wiley-VCH, Berlin (2004). 10.1093/mnras/stx1978.
[17] B.L. Henke, E.M. Gullikson, J.C. Davis, X-ray-interactions: photoabsorption, scattering, transmission, and reflection at E = 50-30,000 eV, Z = 1-92, 1993, 10.1006/ADND.1993.1013.
[18] H.K. Chung, M.H. Chen, W.L. Morgan, Y. Ralchenko, R.W. Lee, FLYCHK: generalized population kinetics and spectral model for rapid spectroscopic analysis for all elements, High Energy Density Phys. 1 (1) (2005), https://doi.org/10.1016/j.hedp.2005.07.001.
[19] S. Fujioka, T. Johzaki, Y. Arikawa, Z. Zhang, A. Morace, T. Ikenouchi, T. Ozaki, T. Nagai, Y. Abe, S. Kojima, S. Sakata, H. Inoue, M. Utsugi, S. Hattori, T. Hosoda, S.H. Lee, K. Shigemori, Y. Hironaka, A. Sunahara, H. Sakagami, K. Mima, Y. Fujimoto, K. Yamanoi, T. Norimatsu, S. Tokita, Y. Nakata, J. Kawanaka, T. Jitsuno, N. Miyanaga, M. Nakai, H. Nishimura, H. Shiraga, H. Nagatomo, H. Azechi, Heating efficiency evaluation with mimicking plasma conditions of integrated fast-ignition experiment, Phys. Rev. E 91 (6) (2015), https://doi.org/10.1103/PhysRevE.91.063102.
[20] S. Fujioka, H. Shiraga, M. Nishikino, M. Heya, K. Shigemori, M. Nakai, H. Azechi, S. Nakai, T. Yamanaka, Penumbral imaging for measurement of the ablation density in laser-driven targets, Rev. Sci. Instrum. 73 (7) (2002) 2588, https://doi.org/10.1063/1.1483899.
[21] V. Goncharov, Theory of the ablative Richtmyer-Meshkov instability, Phys. Rev. Lett. 82 (10) (1999) 2091–2094.
[22] T. Sano, T. Inoue, K. Nishihara, Critical magnetic field strength for suppression of the Richtmyer-Meshkov instability in plasmas, Phys. Rev. Lett. 111 (20) (2013), https://doi.org/10.1103/PhysRevLett.111.205001.
[23] G. Dimonte, B. Remington, Richtmyer-Meshkov experiments on the Nova laser at high compression, Phys. Rev. Lett. 70 (12) (1993), https://doi.org/10.1103/PhysRevLett.70.1806.
[24] R. Holmes, Richtmyer-Meshkov instability growth: experiment, simulation and theory, J. Fluid Mech. 389 (1999) 55–79.
[25] C. Reich, P. Gibbon, I. Uschmann, E. Förster, Yield optimization and time structure of femtosecond laser plasma Kα sources, Phys. Rev. Lett. 84 (21) (2000), https://doi.org/10.1103/PhysRevLett.84.4846.